Modeling "Wrong Side" Failures Caused by Geomagnetically Induced Currents in Electrified Railway Signaling Systems in the UK

C. J. Patterson[1], J. A. Wild[1], and D. H. Boteler[2]

[1]Department of Physics, Lancaster University, Lancaster, UK
[2]Natural Resources Canada, Ottawa, Ontario, Canada

Key Points:

- A model of DC signaling systems on AC-electrified railways has been extended to examine "wrong side" failures caused by space weather
- "Wrong side" failures can occur when these lines are subjected to electric fields that are expected to arise once every one or two decades
- The threshold electric field for "wrong side" failures is lower than for "right side" failures

Corresponding author: Cameron Patterson, `c.patterson2@lancaster.ac.uk`

Abstract

The majority of studies into space weather impacts on ground-based systems focus on power supply networks and oil and gas pipelines. The effects on railway signaling infrastructure remain a sparsely covered aspect even though these systems are known to have experienced adverse effects in the past as a result of geomagnetic activity. This study extends recent modeling of geomagnetic effects on DC signaling for AC-electrified railways in the UK that analyzed "right side" failures in which green signals are turned to red. The extended model reported here allows the study of "wrong side" failures where red signals are turned green: a failure mode that is potentially more dangerous. The results show that the geoelectric field threshold at which "wrong side" failures can occur is lower than for "right side" failures. This misoperation field level occurs on a timescale of once every 10 or 20 years. We also show that the estimated electric field caused by a 1-in-100 year event could cause a significant number of "wrong side" failures at multiple points along the railway lines studied.

Plain Language Summary

Space weather refers to the conditions and variations in the Sun-Earth environment that affect technological infrastructure both in space and on the ground. Previous studies show that railways in various countries have been affected by space weather, whereby geomagnetic interference in signaling systems leads to the display of erroneous signals. The disruption in signaling can happen when geomagnetic disturbances induce electric currents in the rails that interfere with the electrical circuits used to detect trains. This research builds upon an earlier model that assessed the effects of geomagnetically induced currents on railway signaling systems in the United Kingdom, providing the opportunity to examine new failure modes. The results show that "wrong side" failure (the potentially hazardous type of misoperation), where red signals are turned green, can occur in the line when a geomagnetic storm with frequency of about one or two decades occurs. We also demonstrate that a 1-in-100 year extreme event could cause many misoperations throughout the line in both directions of travel.

1 Introduction

Space weather has the potential to affect ground- and space-based infrastructures, causing interference and/or damage. Among the many hazards associated with space weather, geomagnetically induced currents (GICs) are a significant concern. During geomagnetic disturbances, fluctuations of ionospheric and magnetospheric currents cause variations in the magnetic field observed at the Earth's surface. These variations in the magnetic field induce electric currents in the Earth and in long conductors such as power grids (Pirjola, 1985; Boteler & Pirjola, 2019; Lewis et al., 2022), oil and gas pipelines (Pulkkinen et al., 2002; Boteler & Trichtchenko, 2015), and railways (Alm, 1956; Lejdström & Svensson, 1956; Darch et al., 2014; Boteler, 2021).

One example of space weather causing railway signaling issues occurred in Sweden during a geomagnetic storm in July 1982. A signal changed from green to red and back to green even though no train was present on the track or any other fault conditions existed. It was later estimated that the storm induced a geoelectric field of 4-5 $V\,km^{-1}$ (Wik et al., 2009), and the malfunction was explained by GICs flowing through the railway signaling network. Statistical analyses to explore the possible correlation between railway infrastructure misoperations and geomagnetic disturbances revealed a rise in the number of unexplained signal misoperations during periods of high geomagnetic activity, showing links between operational anomalies in railway infrastructure and geomagnetic interference (Kasinskii et al., 2007; Ptitsyna et al., 2008; Eroshenko et al., 2010).

In 2012, severe space weather was added to the UK National Risk Register of Civil Emergencies (Cabinet Office, 2012). Following this, the Department for Transport commissioned a report on the impact of space weather on UK railway infrastructure. This report identified knowledge gaps related to track circuit interference, noting that railway assets, including signaling systems, are potentially vulnerable to the effects of space weather (Darch et al., 2014). To further explore the impacts of space weather on railways and raise awareness among network operators, the European Commission's Joint Research Centre, the Swedish Civil Contingencies Agency, the UK Department for Transport, and the US National Oceanic and Atmospheric Administration jointly organized the "Space Weather and Rail" workshop in 2015, highlighting similar knowledge gaps in this area of study (Krausmann et al., 2015).

Patterson et al. (2023) (from here on referred to as P23) conducted an initial investigation of how DC track circuit signaling systems on AC electrified railways in the United Kingdom are impacted by GICs. The study focused on the simplest case of misoperation, known as "right side" failures, which have the potential to cause disruption, but are not hazardous. The analysis involved building a network model of two UK railway lines (detailed in P23 and summarised in section 3) and applying varying levels of uniform geoelectric field to identify the thresholds for "right side" failure. The study concluded that the return period for an event strong enough to cause "right side" failures would be about once every 30 years, and that a 1-in-100 year event would cause a significant number of misoperations across both lines. The model was built upon earlier work by Boteler (2021). In this paper, we extend the work described above to focus on the potentially hazardous failure mode, known as "wrong side" failures.

Section 2 details the operational principles of track circuit signaling and describes how misoperations may occur. Section 3 provides some background for the model in this study and the modifications made to produce this newest iteration. In Section 4, we provide the results of the modeling. In 4.1 and 4.2, we show the effects of the additions to the model (cross bonds and train axles, respectively) and how they may impact the results; 4.3 gives the threshold electric fields for "wrong side" failures in each block, and 4.4 discusses how those thresholds differ with changes to the leakage to the ground due to weather conditions. Section 4.5 shows examples of the resultant currents through the relays at a range of electric field values from the misoperation threshold to a 1-in-100 year extreme assuming a number of trains spaced along the line.

2 Track Circuit Signaling

Railway technologies and infrastructures are constantly evolving. In the UK, Network Rail's Digital Railway initiative aims to reduce the reliance on track-side signals. For high-capacity intercity lines there is a push to introduce radio-based European Train Control System technology. These newer technologies, and the widespread use of axle counters, may reduce the susceptibility of future signaling systems to GICs and are being rolled out progressively on existing UK main lines. However, this technology is unlikely to be deployed on all lines due to cost and probably not even the majority of lines. Since typical railway infrastructure has a lifetime of 30-40 years, rolling technology upgrades also occur over long timescales. Meanwhile, DC track circuits (of the kind we are modeling) are relatively cheap and there are thousands installed in the UK network that will remain in use for decades to come (Knight-Percival et al., 2020).

The circuit diagram of a DC track circuit for the case of an electrified railway line is shown in Figure 1. Insulated rail joints (IRJs) on one rail (the signaling rail) divide it into blocks, while the other rail (the traction rail) remains unbroken to act as a return path for the traction current that powers the train. At the beginning of each block is a relay, which is powered by a power supply at the other end of the block, with the current traveling through the signaling and traction rails. If there is no train present, the
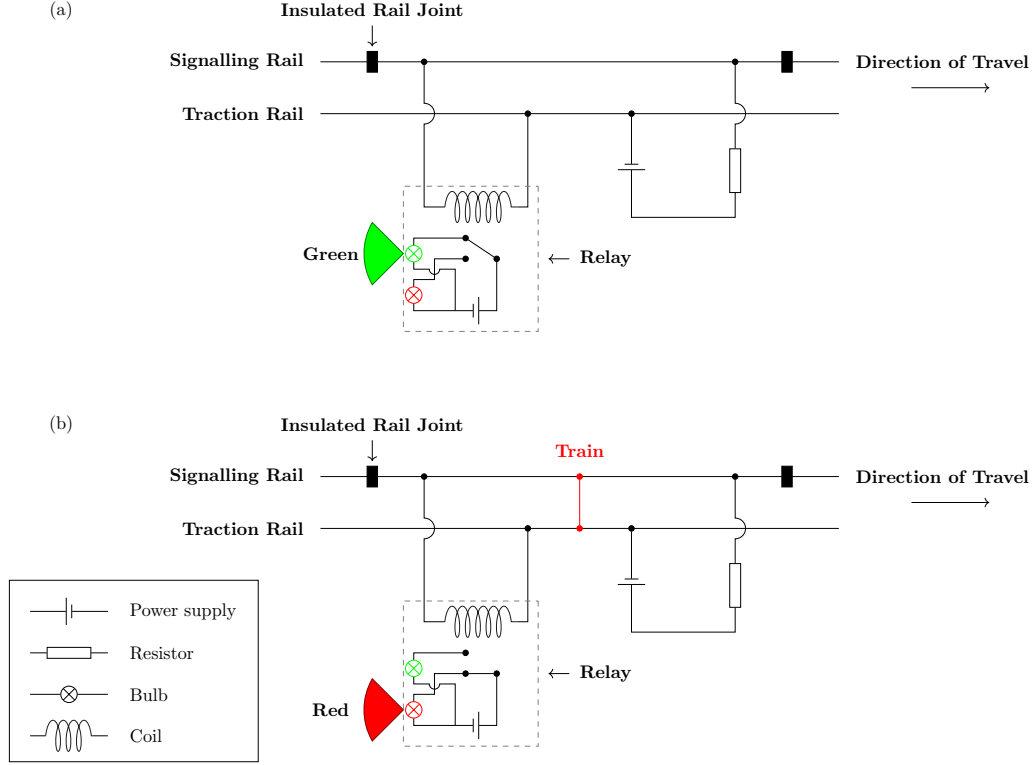
Figure 1. This circuit diagram shows a railway signaling track circuit for a single block within a network when (a) unoccupied, and (b) occupied by a train. The blocks are separated by insulated rail joints in the signaling rail, while the traction rail remains continuous.

current energises the relay and a green signal is displayed, as in (a). However, if a train occupies the block, the current is redirected by the wheels and axle, preventing the relay from energizing and leading to a red signal, as in (b). To operate correctly, the relay requires the current to pass specific thresholds to energise or de-energise. However, this operation can be disrupted by GICs, which can cause "right side" failures, where the energized relay in a block with no train present is de-energized by GICs, or "wrong side" failures, which occur when a de-energized relay in a block with a train present is re-energized, making the block seem clear when it is occupied. On non-electrified railway lines, IRJs are commonly placed in both rails at the same positions. This means that the potential for misoperation due to space weather is lower, as there is equal induction in both rails, meaning no potential difference across the relay (Boteler, 2021). It should also be noted here that the positioning of the relay at the start of the block and the power supply at the end is inverse to the layout described in P23. The industry standard for track circuit design is to have the relay at the start of the block, however when considering "right side" failures (as in P23), because there are no trains present in any blocks, the relative position of the relay and the power supply is arbitrary. When considering "wrong side" failures, the distances from the train to the relay and the power supply are important, so the model has been amended to take this into account.

As the speed of trains has increased over time, the basic, two-aspect, red/green signals have been substituted, where needed, for three-aspect or four-aspect signalling, which give drivers advanced notice of the signal state in the next three or four blocks. This allows them to have sufficient time to safely reduce their speed as they approach a red sig-
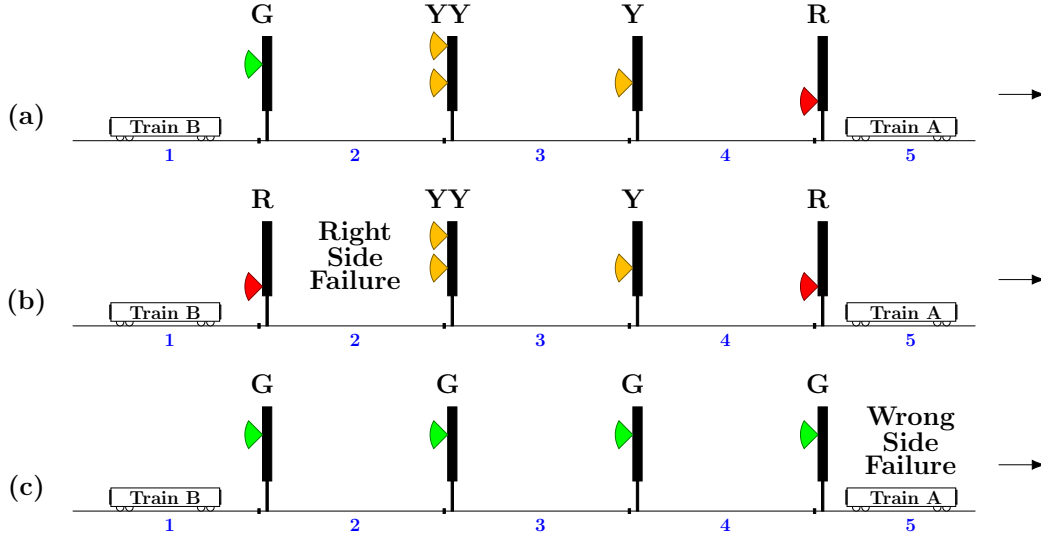
Figure 2. Diagram showing the operation of four-aspect signaling during (a) normal conditions, (b) a "right side" failure in block 2, and (c) a "wrong side" failure in block 5. The direction of travel is left to right.

nal. The state of the yellow signals in three-aspect and four-aspect signaling is determined by the logic of the occupied block ahead, rather than the presence or absence of trains in the previous blocks. Figure 2 demonstrates the principles of four-aspect signalling systems, and how "right side" and "wrong side" failures can impact their operation. The cases shown are to demonstrate how misoperations impact four-aspect signalling, however, only a subset of possible misoperations are shown. In (a), we see normal operation: train A is occupying block 5, the four signals preceding it, from closest to furthest are red (danger/stop) - indicating there is a train occupying the next block, single yellow (caution) - indicating to the driver that they must stop at the next signal, double yellow (preliminary caution) - indicating that the next signal is a single yellow, and green (clear) - the train can proceed normally. If train A remains in block 5, train B would enter block 2 normally, start to slow down in block 3, and slow to a stop in block 4. In (b), a "right side" failure has occurred in block 2: without advanced caution from the single or double yellow signals, the driver of train B now sees the signal change from green to red, meaning they would have to decelerate the train more rapidly than normal to attempt to avoid passing the red signal. In the case of a space weather induced misoperation, there is nothing hazardous in block 2 causing the signal to change, it is the induced currents causing the relay to display the wrong signal. However, the driver does not know this, and the rapid deceleration of the train also has the potential to cause injuries to those on-board. In (c), a "wrong side" failure has occurred in block 5, currently occupied by train A: the driver of train B continues along the line, unaware that block 5 is actually occupied. This is potentially a far more hazardous case, as if the misoperation persists, there is the potential of a collision as train B may not be able to decelerate fast enough to avoid colliding with the rear of train A. Three-aspect signalling uses the same principles described above, but without the double yellow signal.

In this study, the analyses focus on the Glasgow to Edinburgh via Falkirk line, however results are also given for the Preston to Lancaster section of the West Coast Main Line (WCML). Both lines were modeled in P23, and the Glasgow to Edinburgh line has been highlighted due to it being the most susceptible to misoperations of the two, and because the entire line from start to finish is included in the model rather than a sec-
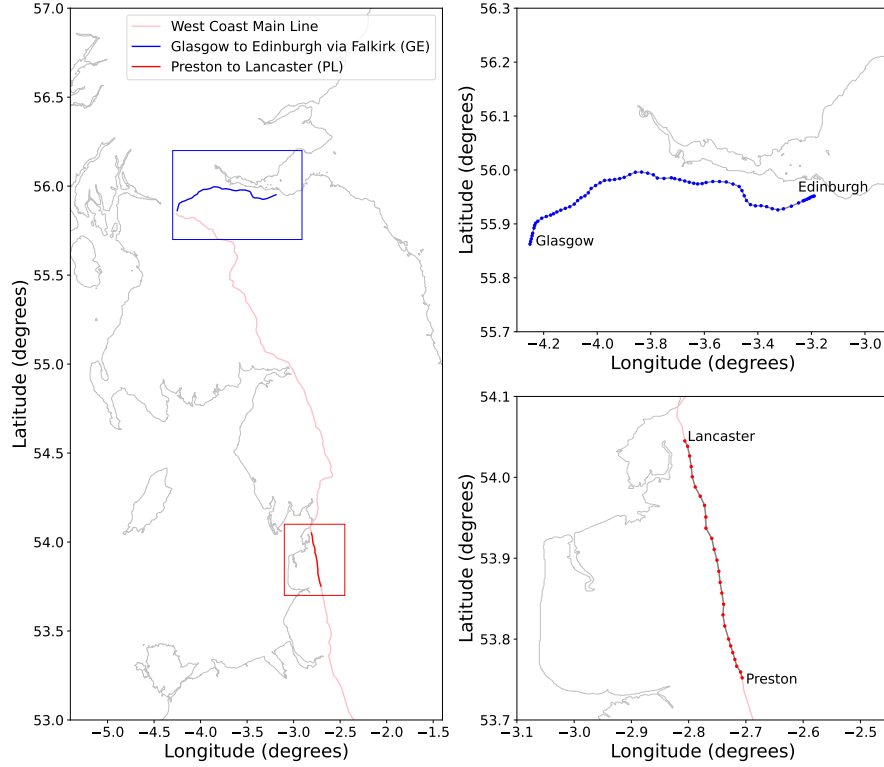
Figure 3. A geographic map of part of the United Kingdom showing the railway lines modelled in this paper, with detailed views showing the location of the track circuit blocks in the top and bottom right. The top (blue) line is the Glasgow to Edinburgh via Falkirk line, orientated in an east-west direction; the bottom (red) line is a north-south orientated section of the West Coast Main Line from Preston to Lancaster, the remainder of the line is shown less opaquely.

tion of a longer line, as is the case with Preston to Lancaster. The Glasgow to Edinburgh line is split into 70 blocks with lengths varying between $0.4-1.9$ km, and the traction rail was calculated to be just over 76 km long. The Preston to Lancaster section of the WCML consists of 25 blocks with lengths varying between $0.8-1.6$ km, and the total traction rail length is not specified as this is a section of a much longer line. It is also worth noting that the Glasgow to Edinburgh line is predominantly east-west orientated, while the Preston to Lancaster section of the WCML is largely north-south orientated. The geographical location and individual track circuit blocks for both lines are shown in Figure 3.

3 Signaling System Modeling

The model used in this study is described in detail in P23. A summary of the modeling techniques is given forthwith, along with details of additions made to the model to better represent a realistic railway signaling system and enable the analysis of "wrong side" failures.

Each rail was first modeled as a transmission line with series impedance and parallel admittance corresponding to the resistance of the rail and the leakage to ground respectively. There is a significant difference between the leakage of the signaling rails and the traction rail, this is due to the signaling rails being fitted with insulating pads which reduce leakage, and the traction rail being bonded to the overhead line masts which increase leakage. Next, the transmission line of each rail was converted to a number of individual equivalent-pi circuits, each representing a single block. The equivalent-pi circuits of adjacent blocks were then combined, with the connection points represented as single nodes, to form a nodal network. To complete the nodal network, the power supply and relay components were added, and this connected both rails together. The impedances in the network were then converted to admittances (Figure 4), and the nodal admittance matrix $[Y]$ was constructed. In $[Y]$ the diagonal terms are equal to the sum of all admittances connected to the node corresponding to that index, and the off-diagonal terms are given by the negative of the admittance between nodes. The admittances between each pair of nodes that are not connected (such as where the IRJs separate the signalling rails) are set at zero. The induced electric field was then added as individual voltage sources distributed between the nodes of each block, and the voltage sources were converted to equivalent current sources, as described below.

The equivalent current sources for the power supply, I_{power}, are calculated using Equation 1, where V_{power} is the power supply voltage and r_{power} is the resistance of the power supply's accompanying resistor.

$$I_{power} = \frac{V_{power}}{r_{power}} \tag{1}$$

The electric field induced in a section of rail is represented in the model by an equivalent current source calculated with Equation 2, where $E_{\parallel}$ is the parallel electric field component to the rail and Z is the series impedance per unit length of the rail.

$$I_E = \frac{E_{\parallel}}{Z} \tag{2}$$

The sum of equivalent current sources directed into each node were then calculated to form $[J]$ (a matrix of nodal equivalent current sources). Equation 3 shows the relationship between $[J]$, the voltages at each node ($[V]$), and the network admittances ($[Y]$).

$$[J] = [Y][V] \tag{3}$$

The nodal voltages can be obtained by inverting the matrix $[Y]$ and multiplying by the nodal equivalent current sources $[J]$, as shown in Equation 4. The potential difference across the relay is given by the difference between the signaling rail and traction rail nodal voltages on either side of the relay, from which the current flowing across the relay can be calculated. The current across the relay is therefore defined as positive when it flows from the signaling rail to the traction rail.

$$[V] = [Y]^{-1}[J] \tag{4}$$

The electrical characteristics of the rails and parameters for track circuit components are summarised in Table 1. For further details please see P23.

3.1 Cross Bonding

Where previously the model considered only a single track (pair of rails) in one direction of travel, now it has been modified to include both directions of track, connected
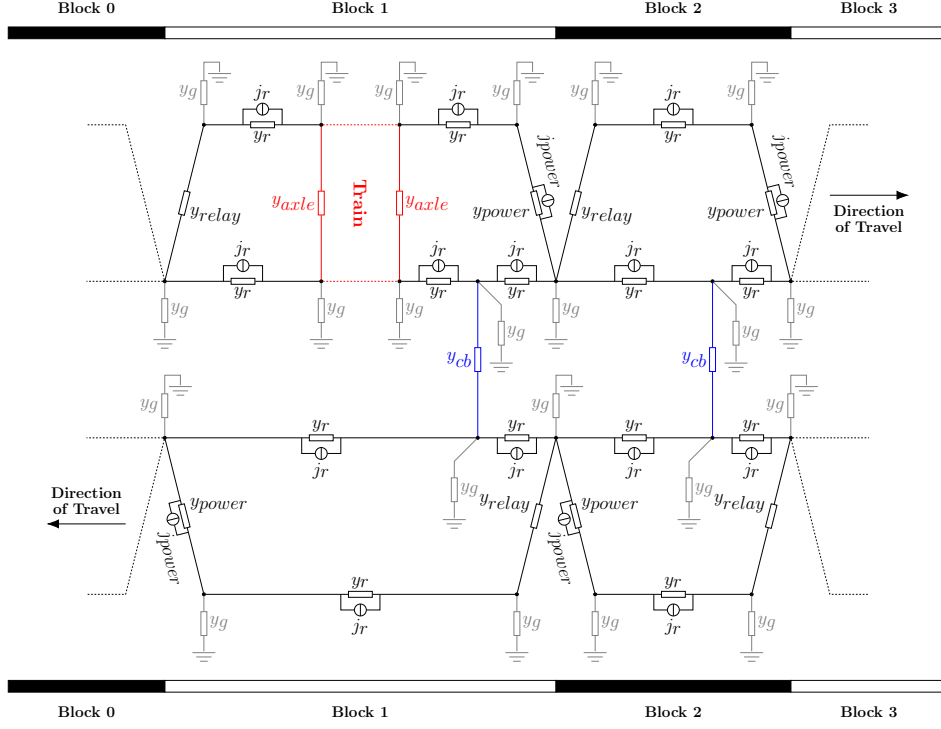
Figure 4. Circuit diagram showing the nodal admittance network of a section of a line with two track circuit blocks in each direction of travel. Track circuit blocks are separated by insulated rail joints in one rail but share a continuous traction rail. The traction rails are periodically connected with cross bonds (shown in blue), and there is a train in the top left block (shown in red). Only the first and last axle of the train is shown here for simplification, but every axle is included in the model. The components making up the network are the current source and admittance of the power supply (j_{power} and y_{power} respectively), the admittance of the relay (y_{relay}), the admittance to the ground at each node (y_g), the admittance due to the rail between nodes, (y_r), the currents induced in the rails due to the geoelectric field between nodes (j_r), the admittance of the cross bond (y_{cb}), and the admittance of the train axles (y_{axle}). Note that the y_g, y_r and j_r are dependent on the length of the segment and the rail's electrical characteristics, and would have varying values.

Table 1. Electrical characteristics of the rails and parameters for track circuit components.

Rail Resistance	$(\Omega \, \mathrm{km}^{-1})$
Signaling rail	0.0289
Traction rail	0.0289
Leakage	$(\mathrm{S} \, \mathrm{km}^{-1})$
Signaling rail (wet)	0.4
Traction rail (wet)	2.0
Signaling rail (moderate)	0.1
Traction rail (moderate)	1.6
Signaling rail (dry)	0.025
Traction rail (dry)	1.530
Track Circuit Parameters	
Power supply	10 (V)
Power supply resistor	7.2 (Ω)
Relay coil resistance	20 (Ω)
Pick-up current	0.081 (A)
Drop-out current	0.055 (A)

by wires with a total admittance of $1000 \, \mathrm{S}$ ($1 \, \mathrm{m}\Omega$) (NR/SP/SIG/50004, 2006) called cross bonds which electrically bond both traction rails every $400 \, \mathrm{m}$ (NR/SP/ELP/21085, 2007). The main purpose of cross bonds is to ensure traction rail continuity, if there is a break in one of the traction rails, the traction return current still has an alternate path to flow. The cross bonds effectively add two new nodes to the network (one in each direction of travel), splitting the traction rail into smaller segments in both directions, and changing the values of y_g and y_r at these nodes and adjacent nodes. As the total number of nodes has increased, the dimensions of [Y] also increases, and the sum of admittances into each node that forms the diagonal elements of [Y] that correspond to the cross bonds have an additional admittance equal to y_{cb}.

3.2 Train Axles

To study "wrong side" failures, the admittances of train axles that connect the signaling and traction rails must be considered. The Glasgow to Edinburgh via Falkirk line mainly uses British Rail Class 385 AT-200 trains built by Hitachi Rail for ScotRail. We have used the three-car set as an example, detailed below, but the model could easily be adapted to other train configurations. Every car has four wheelsets (two at each end) each consisting of two wheels and an axle, and the distances between the axles has been estimated based on specifications given by Iwasaki et al. (2017), and shown in Figure 5. It is assumed that each axle has a resistance (known as the train shunt resistance) of $25.1 \, \mathrm{m}\Omega$ ($39.8 \, \mathrm{S}$) (NR/SP/SIG/50004, 2006). For Preston to Lancaster, we have used the 11-car British Rail Class 390 Pendolino trains, assuming each car has the same axle dimensions as the Class 385 given above. Each axle adds two new nodes to the network (one on the signaling rail and one on the traction rail), splitting both rails into smaller segments, and changing the values of y_g and y_r at these nodes and connecting nodes. As the total number of nodes has increased, the dimensions of [Y] also increase, and the sum of admittances into each node that forms the diagonal elements of [Y] that correspond to the axles now have an additional admittance equal to y_{axle}.
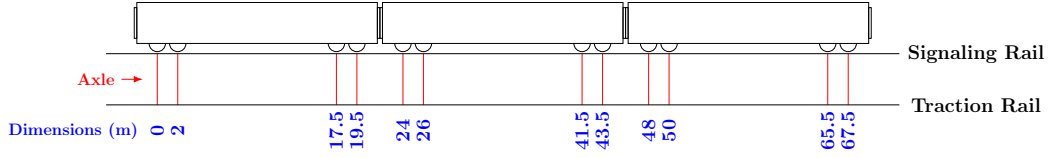
Figure 5. The dimensions of the wheelsets for the three-car British Rail Class 385 AT-200 that is used on the Glasgow to Edinburgh via Falkirk line. The axles (shown in red) electrically connect both rails, as the current travels between the rails through the wheels and axle.

4 Results

4.1 Cross Bonding Effects

To study the effects that cross bonds have on the current through the relays at different magnitudes of geoelectric field strength, we have run the model both with and without the inclusion of cross bonds for 0, 5, and $-5\,\mathrm{V\,km^{-1}}$ and compared the results. Figure 6 shows the current differences through the relays when cross bonds are added. For each relay in the eastwards direction, we see that the current differences are shifted in a positive or negative direction depending on the orientation of the electric field, and this shift is reversed for the opposite direction of travel. We also see that the extent to which the current differences change with electric field strength is less prominent at the ends of the line and more significant at the centre. This is due to the inherent properties of the line shown in P23, and the shorter length of track circuit blocks at both ends of the line, which may not contain a cross bond. When compared with the range of normal current values of -0.5 to $0.5\,\mathrm{A}$, it is apparent that the magnitude of the current differences is very small, so the inclusion of cross bonds has minimal impact on the operation of the track circuits both during normal operation and during a geomagnetic storm. However, cross bonds are still included to ensure the model is as realistic as possible. A similar analysis was undertaken for the effects of axles, but it was found that trains (multiple sets of axles) within a block had no significant impact on the currents in adjacent blocks.

4.2 Distance Along a Block

While investigating the conditions required for "wrong side" failures to occur, it was found that the position of the train in a block is a major factor, as the distance a train has travelled along the block, and hence the lengths of rail between the rear-most axle and the start of the block, will impact the amount of GIC that can affect the relay.

The signal changes as a train moves along the line for the example of two-aspect signaling is shown in Figure 7. Focusing on the middle (blue) block: In Figure 7(a), when a train first enters the block, the signal changes to red as the axles bypass the relay. At this point, the signal in the previous block should also be red, as the train has yet to vacate it completely. In Figure 7(b), the train has moved forward such that it is now completely within the block, the signal behind changes to green as the previous block is now unoccupied. As the train starts moving away from the relay, if there is an external electric field, induction in the rails behind the train starts to drive a current through the relay. Figure 8 shows that because the relay is positioned at the end of the block that the train enters from, the length of rail on the relay side of the train (from which induced currents can reach the relay) increases as the train moves through the block, causing the amount of induced current through the relay to increase as the train progresses. The effect on the current through the relay is shown in Figure 9, where we see that the magnitude of the current increases with both distance travelled through the block and the
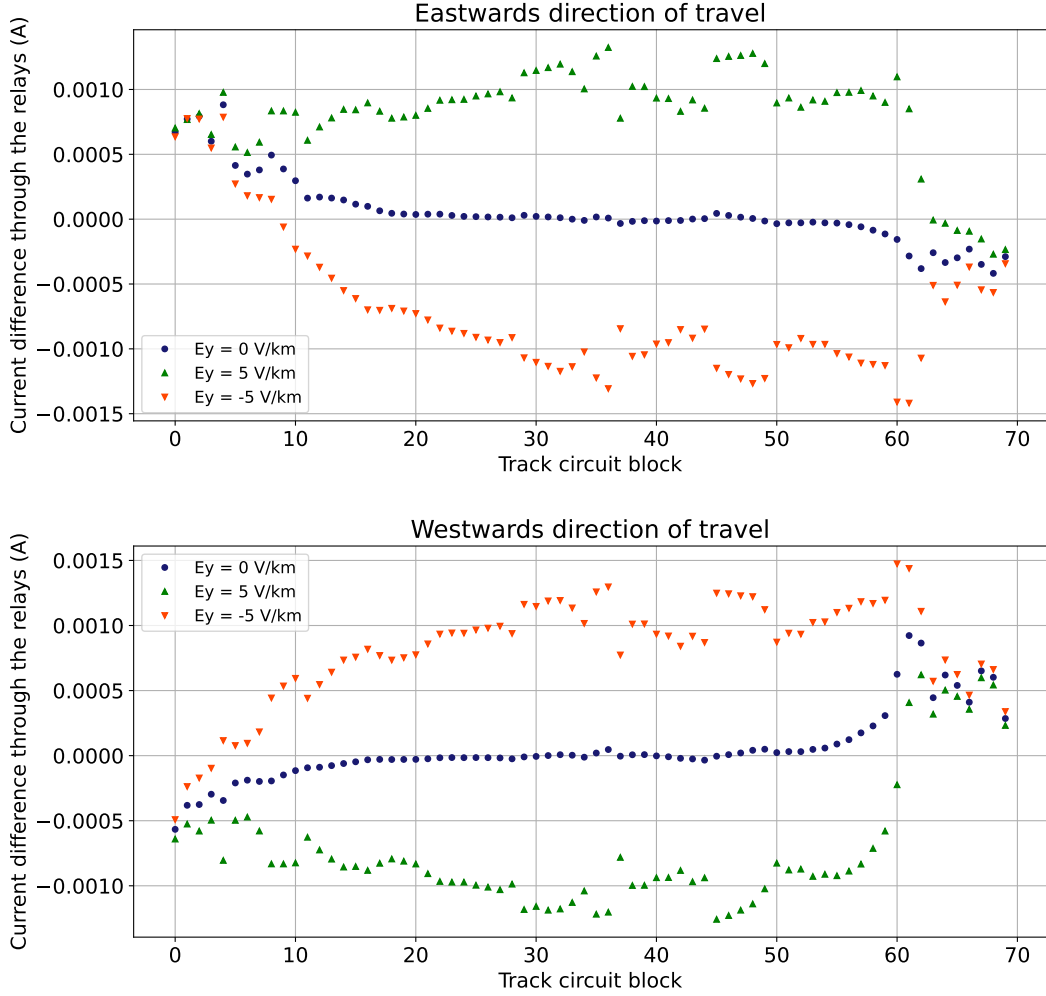
Figure 6. The difference in relay current with and without cross bonds for the Glasgow to Edinburgh via Falkirk line in the eastwards and westwards directions of travel at electric field values of 0, 5, and $-5\,\mathrm{V\,km^{-1}}$. The current differences are shifted in a positive or negative direction depending on the orientation of the electric field, and this shift is reversed for the opposite direction of travel.
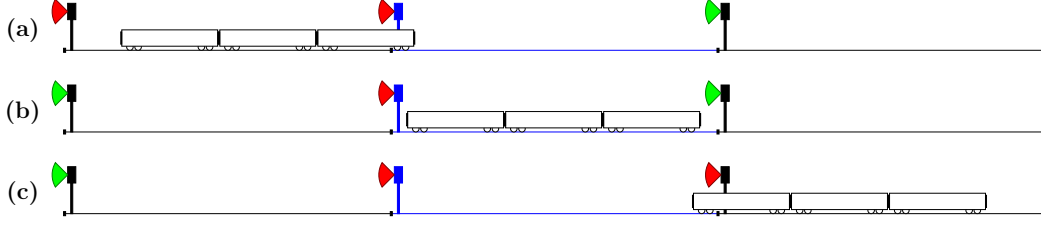
Figure 7. Diagram showing how the signals in a two-aspect system change as a train is travelling along a line. In (a), the train has just entered the block, the signal changes to red as the axles bypass the relay. The signal in the previous block remains red, as it is still occupied by the back end of the train. In (b), the train is now completely within a block, the signal in the previous block changes to green as it is now unoccupied. In (c), almost the entire train has entered the next section, turning the signal for that block red. When the train is positioned at this end of the block, the potential for "wrong side" failure is highest, as it is the maximum distance between the relay and the axles of the train while the train is still occupying the block.
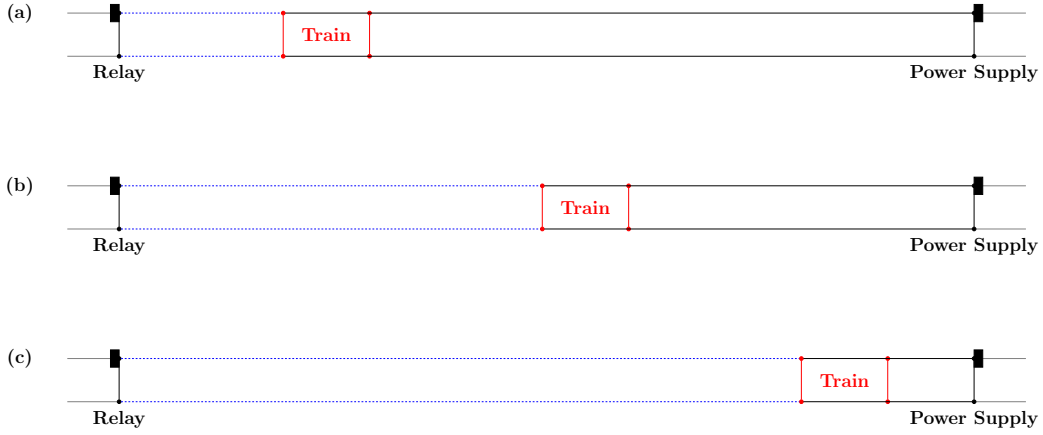

Figure 8. Train axles (indicated by vertical red lines) cut off the power supply current from the relay, effectively splitting the block into two circuits. The number of axles on a train is dependent on the number of carriages, only a single set is shown here for simplicity. In this case, the only source of current reaching the relay is induced in the rails by the electric field. The blue (dashed lines) show the portion of the rails within the relay-side circuit. As the train moves from its position in (a) to (b) to (c), the size of the relay-side circuit grows, and more of the current induced in the rails can reach the relay.

electric field strength applied. Finally, in Figure 7(c), most of the train has passed into the next block, turning the signal for that section red. When the train is in this position, the potential for "wrong side" failure is highest, as it is the maximum distance between the relay and the axles of the train while the train is still occupying the block. It is also worth noting that the unoccupied blocks (with green signals) are potentially vulnerable to misoperations in the form of "right side" failures. In the analyses below, the positions of the trains are always set at the power supply end of the block, i.e., just prior to exiting the block, to model the worst case scenario in terms of positioning that will have the biggest impact on signaling systems.
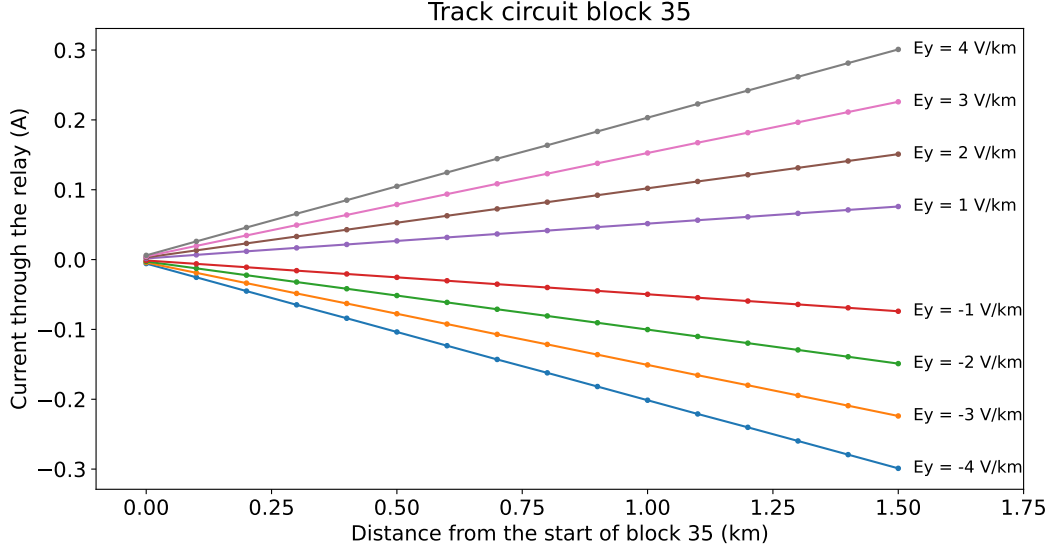
Figure 9. As a train passes through a track circuit block, the magnitude of current across the relay increases. This is due to the distance increase along the block between the axle (which is cutting off the power supply current) and the relay, so more of the rail's induced current is able to reach the relay. The magnitude of the current through the relay also increases with an increased electric field strength.

4.3 Thresholds for "Wrong Side" Failure

To find the thresholds at which "wrong side" failures occur for each block in both directions of travel, increasing values of uniform electric field were applied to each block (eastwards orientated for Glasgow to Edinburgh and northwards orientated for Preston to Lancaster) until the first "wrong side" failure occurred, and the electric field strength at that point was recorded. In this case, the train is at the power supply end of the block to allow the largest amount of induced current to reach the relay. Figure 10 shows the threshold electric field required to trigger a "wrong side" failure in each track circuit block for both directions of travel on the Glasgow to Edinburgh line. The blue crosses indicate the threshold at moderate leakage values, while the blue lines illustrate how the threshold changes with differing leakage in response to environmental conditions, as described in section 4.4. Leakage values for wet, moderate and dry conditions are given in Table 1. For a few track circuit blocks at either end of the line, the thresholds for misoperation are not shown. This is due to these values far exceeding the reasonable value for electric field strengths during space weather events, with some values in the hundreds of volts per kilometer. It is shown that the minimum threshold for "wrong side" failure occurs in track circuit block 36 for both the eastwards and westwards directions of travel with values of $-1.0\,\mathrm{V\,km^{-1}}$ and $1.0\,\mathrm{V\,km^{-1}}$ respectively. This is likely due to its position towards the centre of the line, its long block length, and its almost east-west orientation. Figure 11 shows the results for the Preston to Lancaster section of the WCML, the minimum threshold for "wrong side" failure occurs in track circuit block 6 for northwards and southwards directions of travel with values of $-1.1\,\mathrm{V\,km^{-1}}$ and $1.1\,\mathrm{V\,km^{-1}}$ respectively. The asymmetry between the threshold electric field value at each block in both directions of travel comes from the relative position of the cross bonds within the blocks, and the reversed positioning of the power supply and relay.

As the magnitude of the electric field is increased, the number of blocks that have the potential to experience "wrong side" failures increases, as shown in Figure 12 (ob-
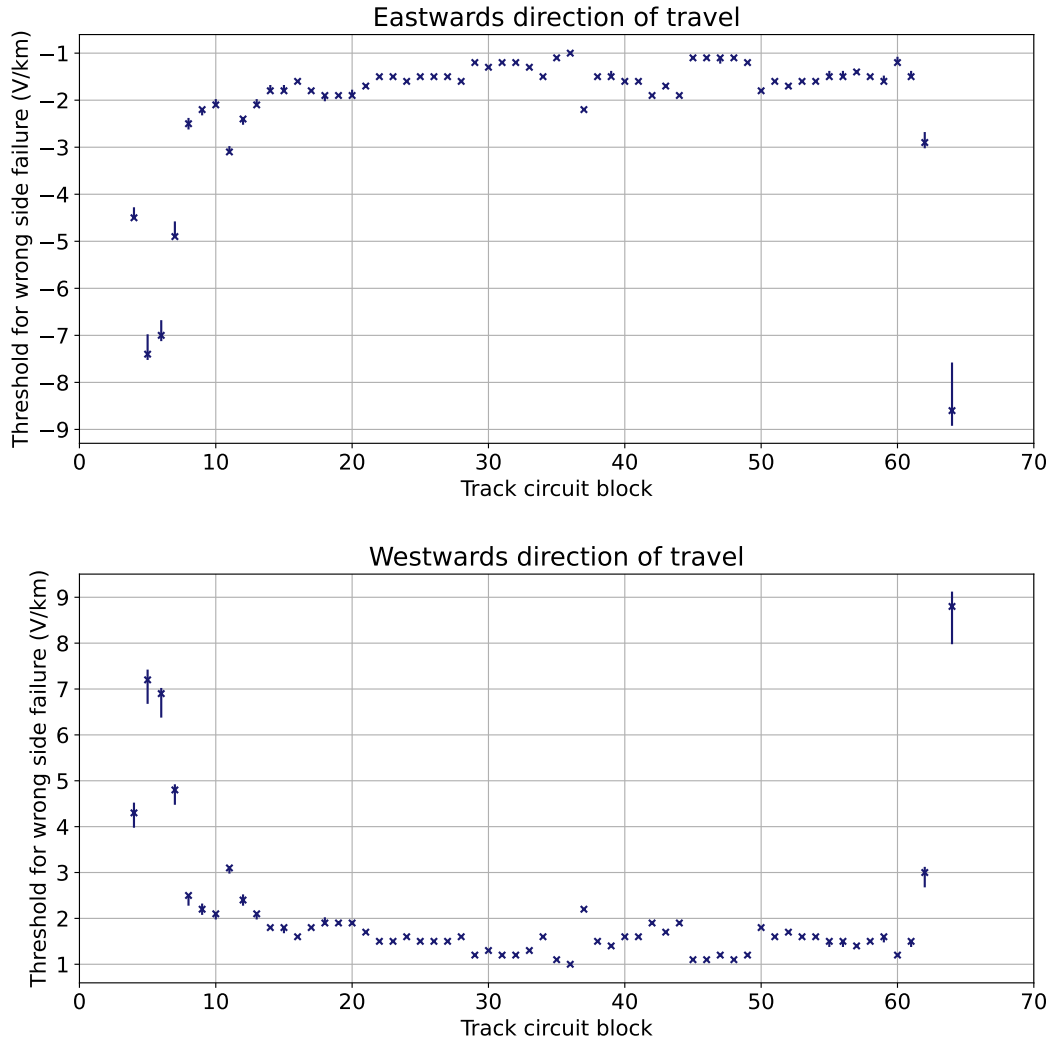
Figure 10. Glasgow to Edinburgh: The threshold west-east electric field values to cause "wrong side" failure for each track circuit block in both eastwards and westwards directions of travel. In both directions of travel, Glasgow is on the left and Edinburgh on the right.
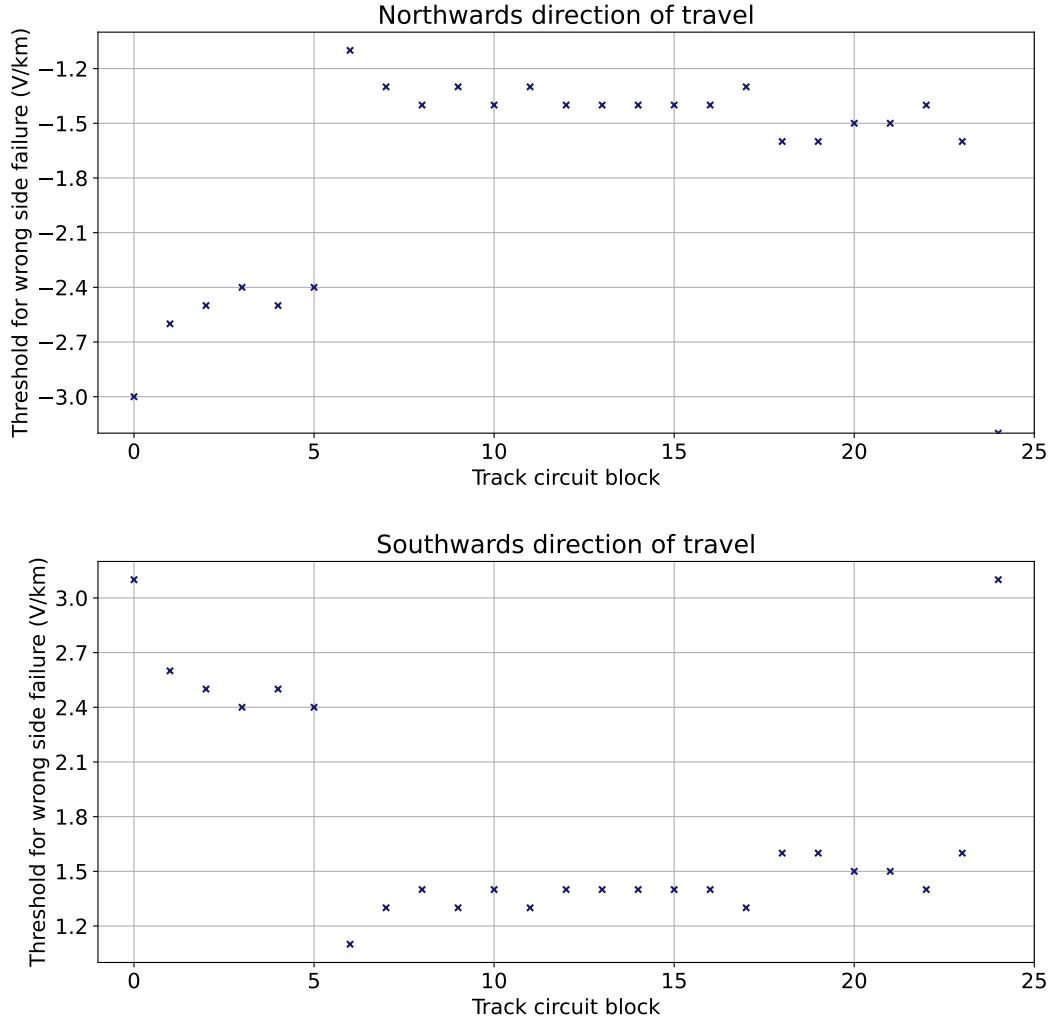
Figure 11. Preston to Lancaster: The threshold south-north electric field values to cause "wrong side" failure for each track circuit block in both northwards and southwards directions of travel.
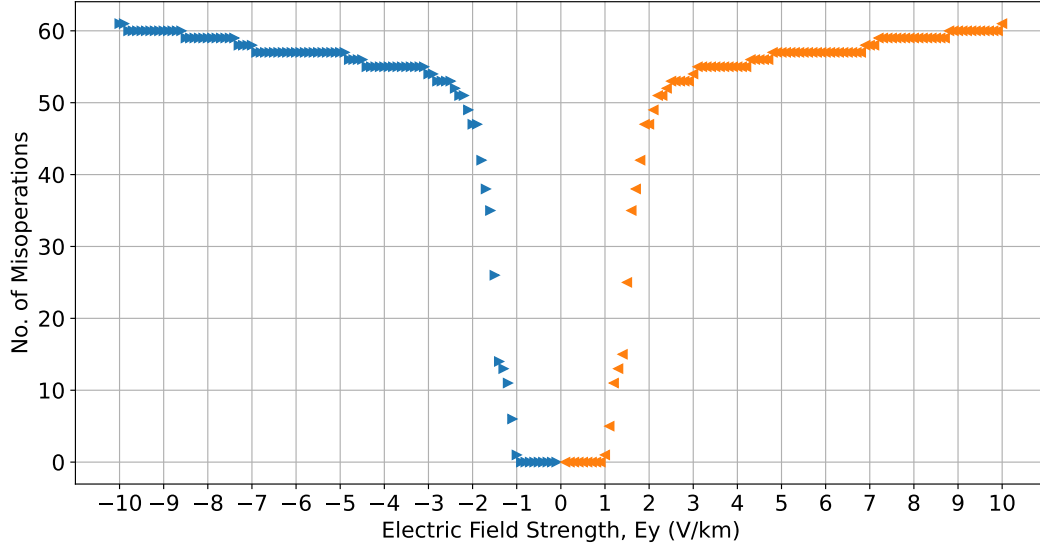
Figure 12. Glasgow to Edinburgh: The number of track circuit blocks with the potential to experience "wrong side" failures at different magnitudes of electric field strength for both the eastwards and westwards directions of travel. The blue (right facing) triangles and the orange (left facing) triangles indicate the eastwards and westwards directions of travel respectively.

tained using Figure 10). This shows the total number of track circuits in the Glasgow to Edinburgh line that have the potential to experience "wrong side" failures for a given electric field strength, regardless of their location within the line. It is important to note that in reality, not all blocks will be occupied by trains at the same time, so this represents a worst case scenario and highlights the number of relays that have the potential to experience "wrong side" failures. In practice, as we explore in Section 4.5, the precise number of "wrong side" failures will depend on the number and distribution of trains on the line as well as the electric field applied. The blue (right facing) triangles indicate the eastwards direction of travel and the orange (left facing) triangles are the westwards direction of travel. Between 1 to $3\,\mathrm{V\,km^{-1}}$ for the westwards direction of travel and -1 to $-3\,\mathrm{V\,km^{-1}}$ for the eastwards direction of travel, there is a steep increase in the number of potential "wrong side" failures, meaning that the threshold for misoperation for most blocks lies within these ranges. Beyond $\pm 3\,\mathrm{V\,km^{-1}}$, larger increase in the magnitude of the electric field strength is needed to cause further potential "wrong side" failures. This is due to multiple factors: (1) some blocks are orientated in such a way that the component of the eastwards electric field parallel to the rails is small, so a larger electric field is needed to induce enough current to cause a misoperation; (2) blocks of shorter length need larger electric fields to induce the currents required to cause a misoperation; (3) the innate properties of the transmission line discussed in P23, which are independent of block length and orientation, cause the current through the relays in blocks at the ends of each line to be more resistant to changes with electric field strength. These factors mean that the threshold for "wrong side" failure in some blocks is much higher, a few of which exceed hundreds of volts per kilometer and are not shown here. We see a similar result for the Preston to Lancaster section of the WCML in Figure 13 (obtained using Figure 11), however, as it is a centre section of the WCML, we do not see the effects of the ends of the line as we do with the Glasgow to Edinburgh line. At $-3.2\,\mathrm{V\,km^{-1}}$ and $3.1\,\mathrm{V\,km^{-1}}$ respectively, all of the relays in the northwards and southwards directions of travel would have the potential to experience "wrong side" failures.
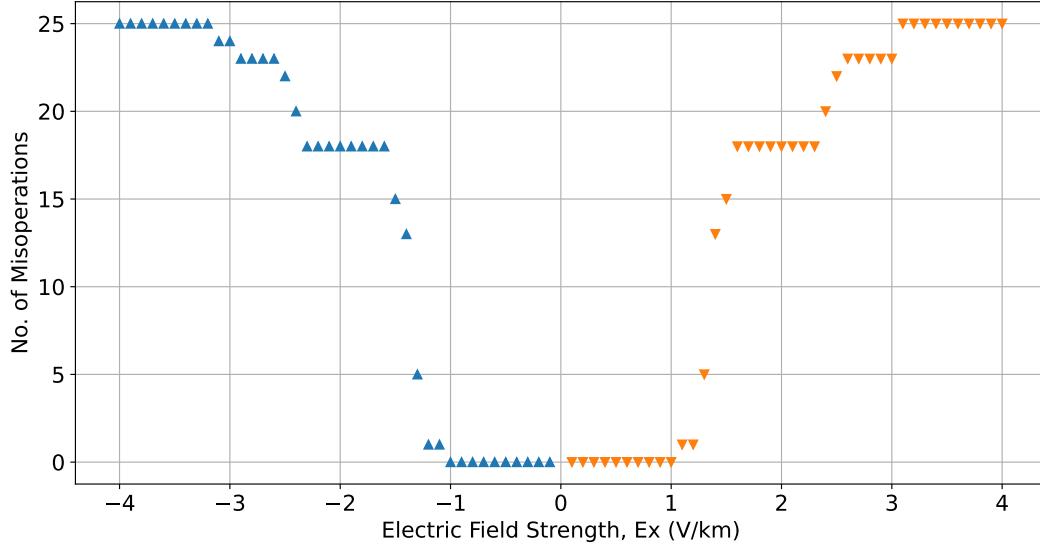
Figure 13. Preston to Lancaster: The number of track circuit blocks with the potential to experience "wrong side" failures at different magnitudes of electric field strength for both the northwards and southwards directions of travel. The blue (up facing) triangles and the orange (down facing) triangles indicate the northwards and southwards directions of travel respectively.

4.4 Effects of Leakage Change

The leakage from the rails to the ground can change with environmental conditions, increasing in wetter weather and decreasing in drier weather. The model was run with leakage values derived from Network Rail standard NR/GN/ELP/27312 (2006), shown in Table 1, to provide a range of "wrong side" failure thresholds. Figure 10 shows that increasing or decreasing the leakage of the rails affects the track circuit blocks towards the ends of the line more than at the centre, this is largely due to the properties of the transmission line. This can be demonstrated by creating a test network of $70{\times}1$ km blocks in each direction of travel with the same orientation (parallel to the electric field direction), each occupied by a train. This makes the results independent of the two other main factors that determine the misoperation thresholds - block length and orientation. In Figure 14, the blue crosses indicate moderate leakage, the orange (upwards) triangles are maximum leakage, and the green (downwards) triangles are minimum leakage. Both directions of travel have an electric field of $E_y = -5\,\text{V}\,\text{km}^{-1}$ applied. The current across the relays in the eastwards direction of travel have increased, possibly driving "wrong side" failures, and the currents across the westwards direction of travel have decreased, which would not lead to "wrong side" failures. This is consistent with the results from Figure 10, which show that negative electric fields can cause "wrong side" failures in the eastwards direction of travel, but not the westwards direction of travel. It is shown that the difference in leakage has a larger impact on the current through the relays that are near the ends of the line when compared with those in the middle, hence the threshold for "wrong side" failures for blocks near the end are more sensitive to changes in leakage due to transmission line properties, and not block length or orientation. This explains why we do not see leakage having an impact on the blocks in the Preston to Lancaster section of the WCML, due to it being a centre part of a longer line.
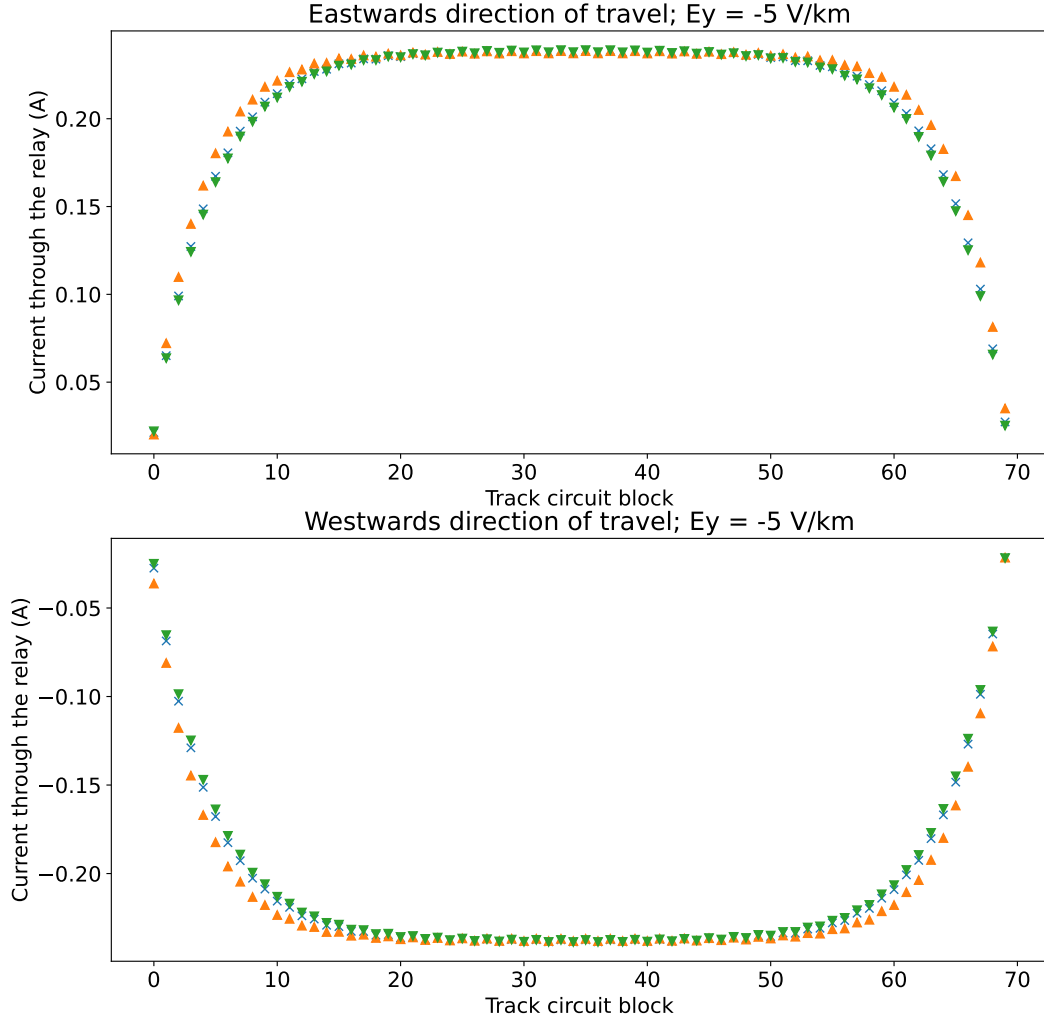
Figure 14. The current through the relays in the eastwards and westwards directions for the $70{\times}1\,\text{km}$ block test network where all blocks are orientated parallel to the direction of the electric field ($E_y = -5\,\text{V}\,\text{km}^{-1}$), and it is assumed that each block is occupied by a train
. The blue crosses indicate moderate leakage, the orange (upwards) triangles are maximum leakage, and the green (downwards) triangles are minimum leakage.

4.5 Applying Uniform Electric Fields

In the following analysis, we have used the example where 7 trains are relatively evenly spaced along the Glasgow to Edinburgh line, and 5 are spaced along the Preston to Lancaster section of the WCML, this is so we can show "right side" failures occurring at the same time as "wrong side" failures. The choice of the number of trains is loosely based on the frequency of trains along those routes, however, this number can differ greatly depending on the density of traffic, which in turn changes depending on the time of day. The number of "wrong side" failures is dependent on how many trains are occupying the blocks and where those occupied blocks are along the line. We use Figure 12 and Figure 13 to quantify the total number of track circuits that have the potential to experience "wrong side" failures given the previously stated assumptions that trains are near the ends of the blocks for both the Glasgow to Edinburgh line and the Preston to Lancaster section of the WCML in the analysis that follows.

4.5.1 Threshold Value

Figures 15 (a) and (b) show the current through the relay of each track circuit block in the eastwards and westwards directions of travel of the Glasgow to Edinburgh line, respectively, assuming no external electric field is applied and 7 trains in each direction. The red (solid) line is the 'drop-out current' the value below which the current must drop to de-energise the relay, turning the signal red; the green (dashed) line is the 'pick-up current', the value above which the current must rise to energise the relay, turning the signal green. A green ring with no fill indicates an unoccupied block operating normally, and a red triangle with no fill is an occupied block operating normally, with the direction of the triangle showing the direction of travel (right for eastwards and left for westwards). It can be seen that under these conditions, all relays are operating normally. The threshold electric field value at which "wrong side" failures begin to occur is shown in the bottom two panels, $E_y = -1.0\,\mathrm{V\,km^{-1}}$ for eastwards (c), and $E_y = 1.0\,\mathrm{V\,km^{-1}}$ for westwards (d). In both directions of travel, block 36 experiences the first "wrong side" failure, which is indicated by a filled green triangle. Figure 16 shows the same results for Preston to Lancaster but assuming 5 trains in each direction, with the direction of the triangle showing the direction of travel (right for northwards and left for southwards). The threshold electric field value at which "wrong side" failures begin are $E_x = -1.1\,\mathrm{V\,km^{-1}}$ for northwards (c), and $E_x = 1.1\,\mathrm{V\,km^{-1}}$ for southwards (d), occurring in block 6 in both cases.

4.5.2 Known Misoperation Value

The magnitude of the electric field known to have caused signaling misoperations in the past in Sweden is estimated to be around $4\,\mathrm{V\,km^{-1}}$ (Wik et al., 2009). With an electric field of this strength applied, Figure 17 shows the example for the Glasgow to Edinburgh line, where both types of misoperation ("wrong side" failures and "right side" failures) occur. According to Figure 12, 55 blocks have the potential to experience a "wrong side" failure for both eastwards at $E_y = -4\,\mathrm{V\,km^{-1}}$ and westwards at $E_y = 4\,\mathrm{V\,km^{-1}}$. As for "right side" failures, we see 16 blocks for eastwards at $E_y = 4\,\mathrm{V\,km^{-1}}$ and 12 blocks for westwards at $E_y = -4\,\mathrm{V\,km^{-1}}$. Figure 18 shows the cases for the Preston to Lancaster section of the WCML, where, according to Figure 13, 25 blocks have the potential to experience a "wrong side" failure for both northwards at $E_x = -4\,\mathrm{V\,km^{-1}}$ and southwards at $E_x = 4\,\mathrm{V\,km^{-1}}$. As for "right side" failures, we see all 5 occupied blocks misoperating in both cases.

4.5.3 1-in-100 Year Extreme Estimate

If we apply the estimate for a 1-in-100 year extreme geoelectric field for the UK, estimated by Beggan (2015) to be approximately $5\,\mathrm{V\,km^{-1}}$, the examples are shown in
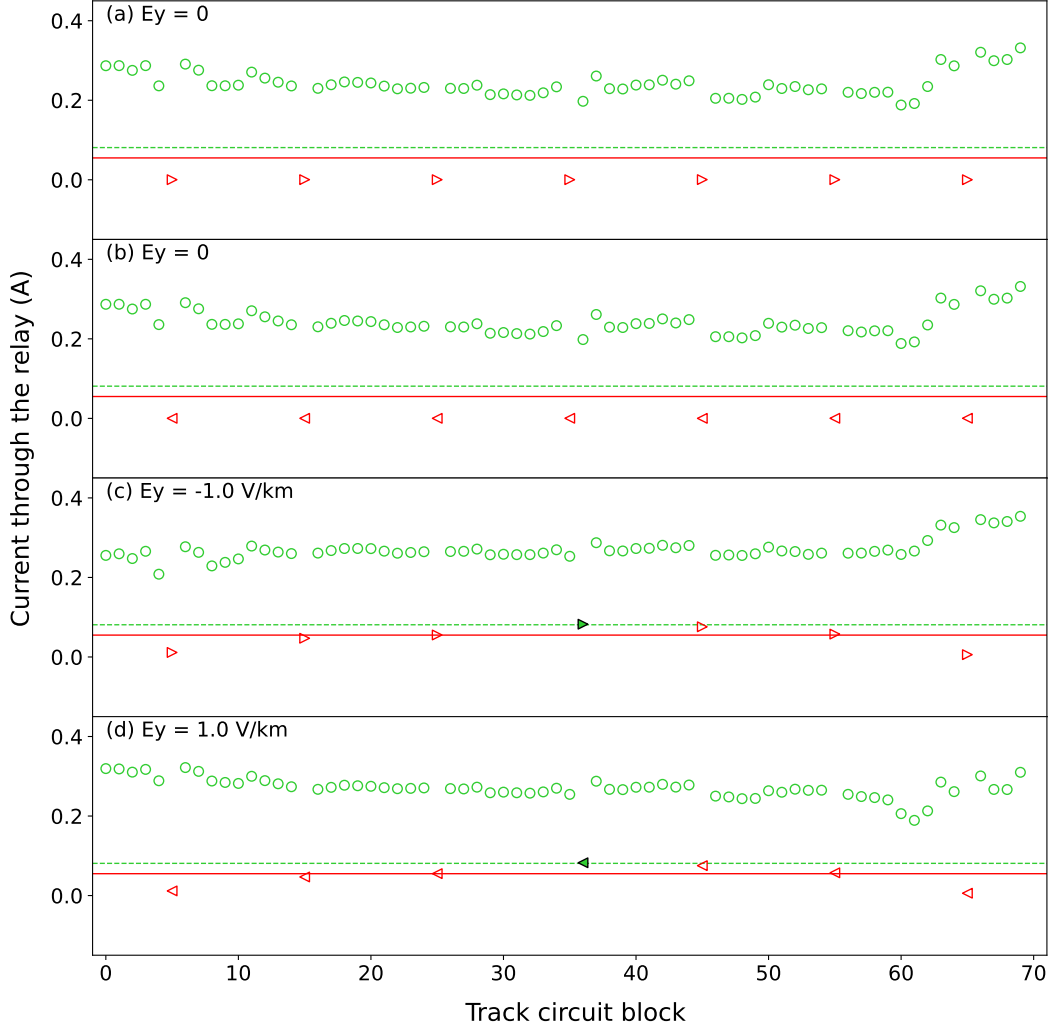
Figure 15. Glasgow to Edinburgh: The current through each relay when no electric field is applied for the eastwards (a) and westwards (b) directions of travel, and at the threshold for "wrong side" failure in the (c) eastwards and (d) westwards directions of travel. The red (solid) line is the 'drop-out current' the value below which the current must drop to de-energise the relay, turning the signal red; the green (dashed) line is the 'pick-up current', the value above which the current must rise to energise the relay, turning the signal green. A green ring with no fill indicates an unoccupied block operating normally, and a red triangle with no fill is an occupied block operating normally, with the direction of the triangle showing the direction of travel (right for eastwards and left for westwards). A filled green triangle indicated a "wrong side" failure. With no electric field applied, all relays are operating normally. At the threshold for "wrong side" failure, we see one misoperation in either direction of travel.
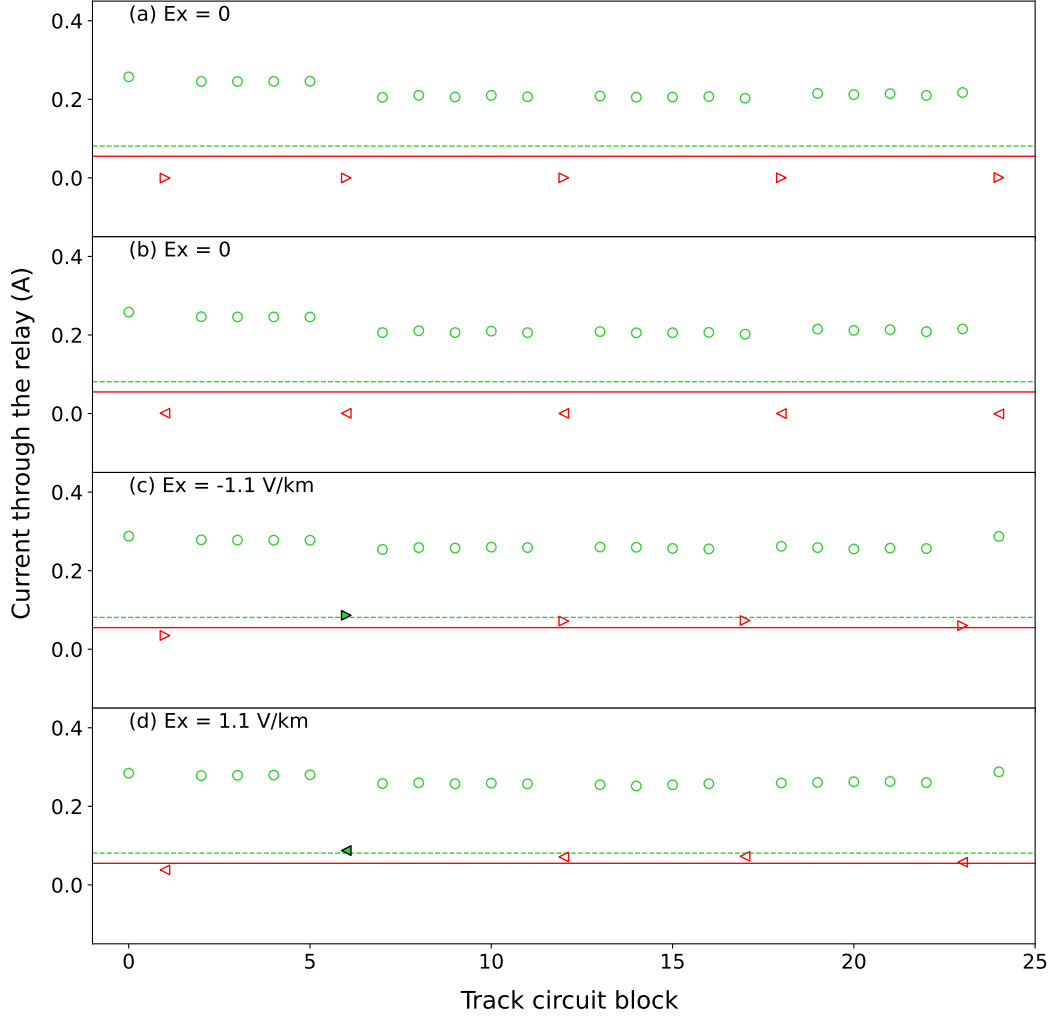
Figure 16. Preston to Lancaster: The current through each relay when no electric field is applied for the northwards (a) and southwards (b) directions of travel, and at the threshold for "wrong side" failure in the (c) northwards and (d) southwards directions of travel. The red (solid) line is the 'drop-out current' the value below which the current must drop to de-energise the relay, turning the signal red; the green (dashed) line is the 'pick-up current', the value above which the current must rise to energise the relay, turning the signal green. A green ring with no fill indicates an unoccupied block operating normally, and a red triangle with no fill is an occupied block operating normally, with the direction of the triangle showing the direction of travel (right for northwards and left for southwards). A filled green triangle indicated a "wrong side" failure. With no electric field applied, all relays are operating normally. At the threshold for "wrong side" failure, we see one misoperation in either direction of travel.
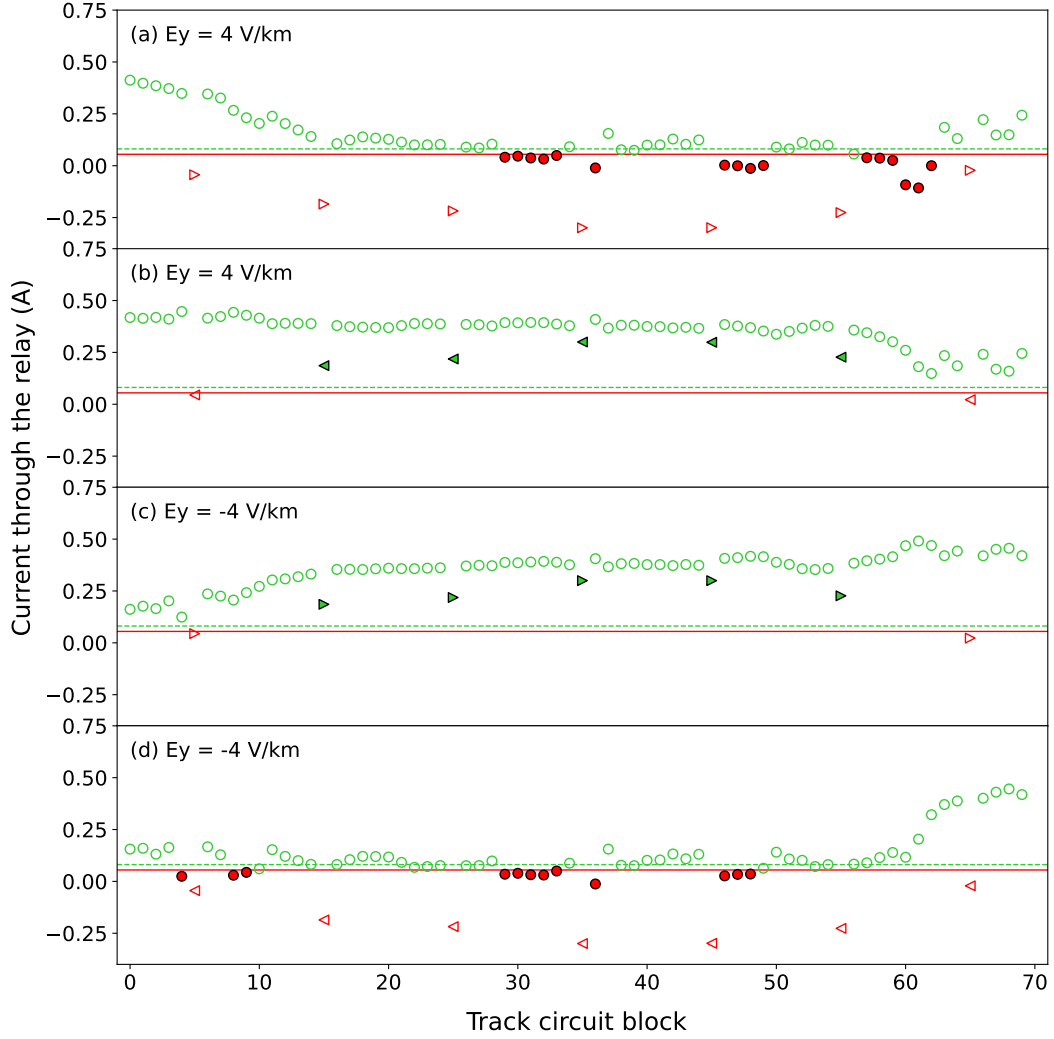
Figure 17. Glasgow to Edinburgh: The current through each relay at $E_y = 4 \, \mathrm{V \, km^{-1}}$ in the (a) eastwards and (b) westwards directions of travel, and at $E_y = -4 \, \mathrm{V \, km^{-1}}$ in (c) eastwards and (d) westwards directions of travel. The red (solid) line is the 'drop-out current' the value below which the current must drop to de-energise the relay, turning the signal red; the green (dashed) line is the 'pick-up current', the value above which the current must rise to energise the relay, turning the signal green. A green ring with no fill indicates an unoccupied block operating normally, and a red triangle with no fill is an occupied block operating normally, with the direction of the triangle showing the direction of travel (right for eastwards and left for westwards). A filled green triangle indicated a "wrong side" failure, and a filled red circle is a "right side" failure. Here we see both types of misoperation occurring in both directions depending on the orientation of the electric field.
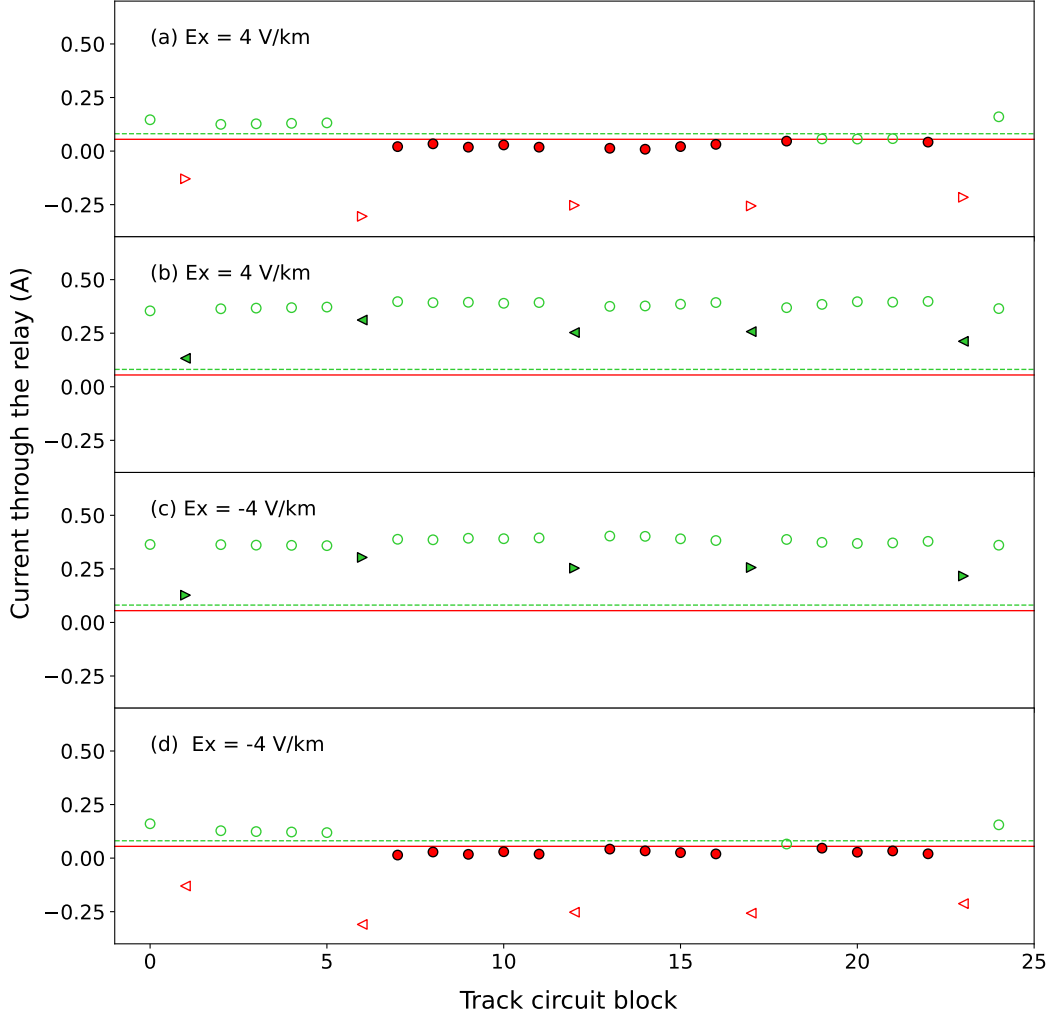
Figure 18. Preston to Lancaster: The current through each relay at $E_x = 4\,\mathrm{V\,km^{-1}}$ in the (a) northwards and (b) southwards directions of travel, and at $E_x = -4\,\mathrm{V\,km^{-1}}$ in (c) northwards and (d) southwards directions of travel. The red (solid) line is the 'drop-out current' the value below which the current must drop to de-energise the relay, turning the signal red; the green (dashed) line is the 'pick-up current', the value above which the current must rise to energise the relay, turning the signal green. A green ring with no fill indicates an unoccupied block operating normally, and a red triangle with no fill is an occupied block operating normally, with the direction of the triangle showing the direction of travel (right for northwards and left for southwards). A filled green triangle indicated a "wrong side" failure, and a filled red circle is a "right side" failure. Here we see both types of misoperation occurring in both directions depending on the orientation of the electric field.

Figure 19. According to Figure 12, the number of track circuits that could potentially experience a "wrong side" failure increases slightly from the from $\pm 4\,\mathrm{V\,km^{-1}}$ value to 56 blocks for eastwards at $E_y = -5\,\mathrm{V\,km^{-1}}$ and 57 blocks for westwards at $E_y = 5\,\mathrm{V\,km^{-1}}$. This is due to the relays towards the ends of the line having much higher thresholds and most relays having already misoperated between ± 1 to $3\,\mathrm{V\,km^{-1}}$. We do see an increase in the number of "right side" failures, with over a third of unoccupied blocks misoperating in both directions of travel. For the examples of Preston to Lancaster in Figure 20, the number of track circuits that could potentially experience a "wrong side" failure cannot increase any further, as the threshold misoperation value for each track circuit had already been reached for both directions of travel at $\pm 4\,\mathrm{V\,km^{-1}}$. However, we do see an increase in the number of "right side" failures occurring in both directions of travel, with nearly all relays experiencing misoperation. The results for "right side" failures agree with P23. It is apparent that a 1-in-100 year extreme event could result in a significant number of signal misoperations.

5 Discussion

The model used in this study builds upon the work set out in P23. With the addition of cross bonds linking together both directions of travel in the line, and train axles to allow the study of "wrong side" failures, we further improve the realism of the model, and the scope of the investigation into the impacts of space weather on railway signaling systems in the UK. The continued usage of Network Rail standards documents ensures we are using appropriate parameters for the UK case, but even the UK network is not homogeneous, so the model is designed to be easily adapted to different rail and track circuit parameters. The model could therefore be used to study railway networks in other countries also with minimal effort provided the data is easily accessible, which is not always the case.

The statistics of electric field and horizontal magnetic field changes reported by Beggan et al. (2013) and Rogers et al. (2020) suggest that the threshold at which "wrong side failures would occur (around $\pm 1\,\mathrm{V\,km^{-1}}$) is exceeded in events that arise once every 10-20 years. Comparing the threshold electric field to cause "wrong side" failures in this study to the threshold for "right side" failures in P23, it is apparent that the strength of the electric field needed to cause a "wrong side" failure is lower than is needed to cause a "right side" failure provided the conditions described above are met. To cause a "wrong side" failure, due to the train axles cutting off the power supply, the current flowing through the relay is almost entirely the induced current from the electric field. However, in the case of "right side" failure, for the induced current to de-energise the relay, it must overcome the current already present in the circuit from the power supply. It is this difference in current that is responsible for the different threshold values for misoperation.

While it is important to consider the electric field strength threshold for "wrong side" failures, at the same time we need to consider the conditions that need to be met for these misoperations to occur and consider their likelihood. Firstly, a train must occupy the block in question, this might not always be the case, as peak electric fields generated during a geomagnetic storm may occur overnight when traffic is less dense. Secondly, the train must be sufficiently far along the line, such that the distance between the rear axle of the train and the relay is sufficient to build up the required amount of current to cause a "wrong side" failure".

It is challenging to determine which type of misoperation is dominant. The thresholds for "wrong side" failures are lower, but they depend on the multiple factors described above happening simultaneously for misoperation to take place. In contrast, the conditions for right-side failures to occur are simpler, but a higher electric field strength is needed for misoperation to occur.
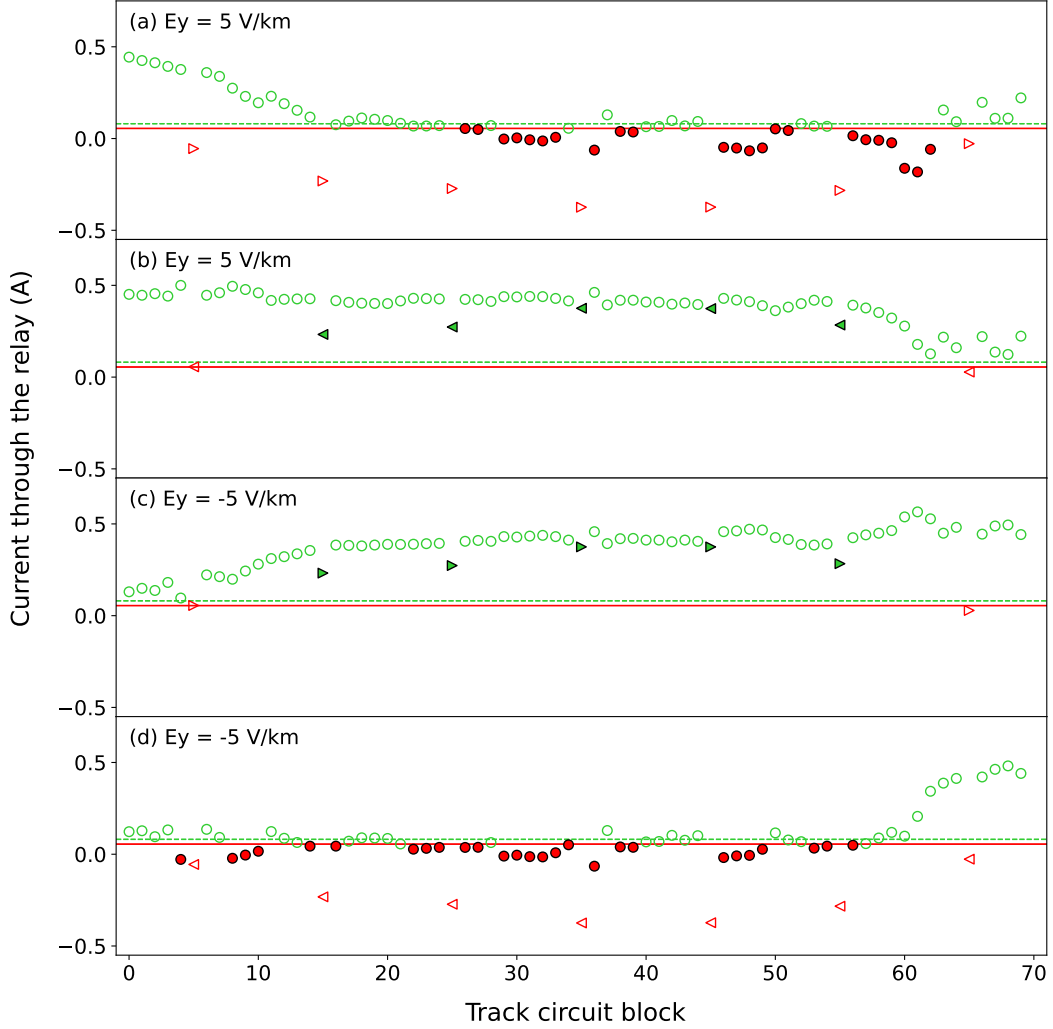
Figure 19. Glasgow to Edinburgh: The current through each relay at the 1-in-100 year extreme geoelectric field estimate of $E_y = 5\,\mathrm{V\,km^{-1}}$ in the (a) eastwards and (b) westwards directions of travel, and $E_y = -5\,\mathrm{V\,km^{-1}}$ in (c) eastwards and (d) westwards directions of travel. The red (solid) line is the 'drop-out current' the value below which the current must drop to de-energise the relay, turning the signal red; the green (dashed) line is the 'pick-up current', the value above which the current must rise to energise the relay, turning the signal green. A green ring with no fill indicates an unoccupied block operating normally, and a red triangle with no fill is an occupied block operating normally, with the direction of the triangle showing the direction of travel (right for eastwards and left for westwards). A filled green triangle indicated a "wrong side" failure, and a filled red circle is a "right side" failure. Here we see both types of misoperation occurring in both directions depending on the orientation of the electric field.
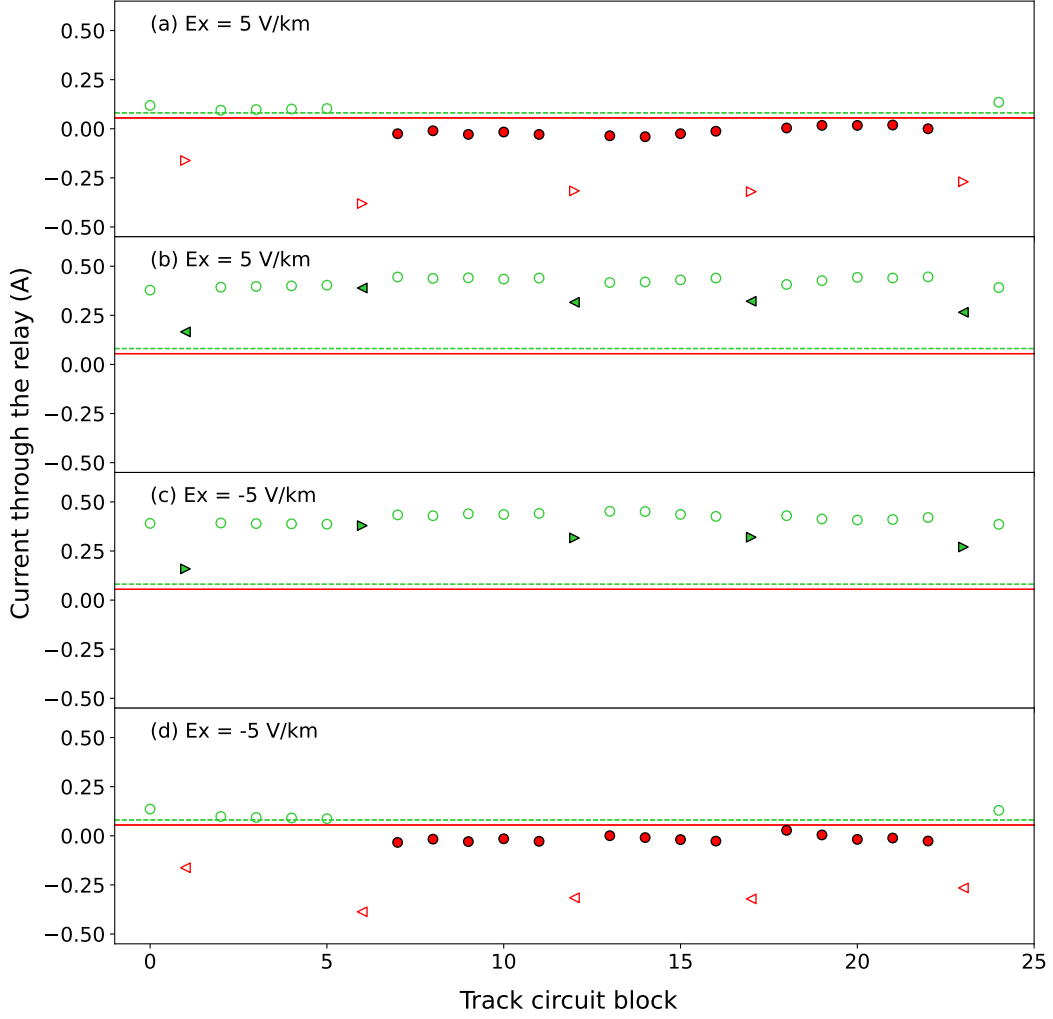
Figure 20. Preston to Lancaster: The current through each relay at the 1-in-100 year extreme geoelectric field estimate of $E_x = 5\,\mathrm{V\,km^{-1}}$ in the (a) northwards and (b) southwards directions of travel, and $E_x = -5\,\mathrm{V\,km^{-1}}$ in (c) northwards and (d) southwards directions of travel. The red (solid) line is the 'drop-out current' the value below which the current must drop to de-energise the relay, turning the signal red; the green (dashed) line is the 'pick-up current', the value above which the current must rise to energise the relay, turning the signal green. A green ring with no fill indicates an unoccupied block operating normally, and a red triangle with no fill is an occupied block operating normally, with the direction of the triangle showing the direction of travel (right for northwards and left for southwards). A filled green triangle indicated a "wrong side" failure, and a filled red circle is a "right side" failure. Here we see both types of misoperation occurring in both directions depending on the orientation of the electric field.

The study has centered on geoelectric fields that have a fixed direction and magnitude, although in actuality, they tend to fluctuate in intensity and direction over time. The effects of time-varying fields requires further investigation. Firstly, changes in electric field direction will have significant impact on the component of the electric field that is parallel to the rails at each track circuit block, either increasing or reducing the level of induced currents in each over time. Secondly, the duration that geoelectric fields maintain a particular strength and/or orientation will determine whether a misoperation is a single event or a series of events. It would also be necessary to analyze the response times of different track circuit types to changes in current to determine whether the relay could respond quickly enough to rapid changes in current, though most track circuit relays are designed to react to changes in current on the millisecond scale, far faster than the resolution of electric field data would allow to be studied (NR/BR/939A, 1971). A detailed study of the impacts of time-varying electric fields on UK railway signaling is beyond the scope of this paper, as this study focuses on the theory and modeling of "wrong side" failures. However, future work in this area would further enhance understanding of the impacts of space weather on railway signaling systems.

A potential next step would be to experimentally confirm the results of the modeling. This could be achieved by placing equipment within the track circuit system to monitor and record current levels. As the ability to forecast space weather events is limited, the equipment would likely have to remain in place for an extended period of time to capture moderate to strong events. The feasibility of placing additional equipment into a mainline railway's systems also depends on whether authorisation from the relevant rail operators and regulators could be obtained. Assuming that it is impractical for monitoring equipment to be installed in all track circuits, then the modeling techniques we have demonstrated in this study could be used to identify the optimal deployment of monitoring instruments. An alternative could be to perform a statistical survey similar to the aforementioned Kasinskii et al. (2007); Ptitsyna et al. (2008); Eroshenko et al. (2010), where a comparison is made between geomagnetic activity and signaling misoperations. One of the challenges with this is that it is assumed that space weather related signaling misoperations would not be recorded as such, as space weather is not a generally well-known cause of signaling issues among railway engineers. This means the study would likely need to be based on whether the total number of misoperations increases during space weather events, rather than relying on the reporting personnel correctly identifying space weather as the specific issue.

It is also important to point out that in the event of severe space weather, railway signaling will not be the only system affected. Power supply networks, communications, Global Navigation Satellite Systems (GNSS) are all susceptible, many of which will also impact the safe and smooth operation of the railway network, regardless of the countless affects to other areas. Further study needs to focus on the connectivity of these systems, and how sectors as a whole could be affected by the loss of interdependent systems (Darch et al., 2014; Hapgood et al., 2021).

6 Conclusion

This study shows the results of a realistic model of geomagnetic interference in DC signaling systems on AC-electrified railway lines. Built upon the model detailed in P23, we now have the ability to study both directions of travel simultaneously, electrically bonded with cross bonds, and to consider "wrong side" failures - when train axles bypass the relays, de-energising them, but geomagnetically induced currents cause the relays to reenergise and display the wrong signal. It is assumed that in blocks that are occupied by trains, the trains are positioned near the end of each block such that GICs would have the maximum impact. This paper also discusses the total number of blocks that could potentially experience "wrong side" failure, this indicates the total number of suscep-

tible blocks rather than the number of "wrong side" failures that would actually be observed, as not all blocks would be occupied by trains.

We have shown that the susceptibility of a track circuit to experience a "wrong side" failure is strongly dependent on the location of the train within the track circuit block, where the risk of misoperation increases as the distance between the train and the relay increases.

It was found that the threshold electric field strength for "wrong side" failure along the Glasgow to Edinburgh line was $E_y = -1.0\,\mathrm{V\,km^{-1}}$ for the eastwards direction of travel and $E_y = 1.0\,\mathrm{V\,km^{-1}}$ for the westwards direction of travel. For the Preston to Lancaster section of the WCML, the threshold electric field strength for "wrong side" failure was $E_x = -1.1\,\mathrm{V\,km^{-1}}$ for the northwards direction of travel and $E_x = 1.1\,\mathrm{V\,km^{-1}}$ for the southwards direction of travel. These correspond to estimates for the electric field strength of events that occur once in a decade or two. The "wrong side" failure threshold electric field strength is lower than the threshold for "right side" failure along the same line.

A uniform electric field with a magnitude of $4\,\mathrm{V\,km^{-1}}$, a value that is known to have caused on Swedish railways in the past, was applied to both routes studied, with 55 of the 70 track circuits on the Glasgow to Edinburgh line, and all of the track circuits on the Preston to Lancaster section of the WCML having the potential to experience "wrong side" failures if occupied by a train. It was also shown that there would be both "wrong side" and "right side" failures in opposite directions of travel.

Applying an electric field with a magnitude of $5\,\mathrm{V\,km^{-1}}$, which is the estimate for a 1-in-100 year extreme event in the UK, the model showed that, for the Glasgow to Edinburgh line, the total number of track circuits with the potential to experience "wrong side" failures increased very slightly from the $4\,\mathrm{V\,km^{-1}}$ value, while the number of "right side" failures increased a greater extent. For the Preston to Lancaster section of the WCML, the number of potential "wrong side" failures has already peaked at the $4\,\mathrm{V\,km^{-1}}$ value, with the number of "right side" failures increasing slightly.

7 Open Research

Network Rail standard documents can be obtained from `global.ihs.com`. Data used for modeling are available from Patterson et al., 2023 (b) `doi.org/10.17635/lancaster/researchdata/633`.

References

Alm, E. (1956). Measures against geomagnetic disturbances in the entire dc track circuit for automatic signalling systems, original publication (in swedish) appendix 5f, betänkande: angående det tekniska utförandet av signalanläggningar vid statens järnvägar, 1956. Translation (in English), June 2020. *Infrastructure Resilience Risk Reporter*, *1*, 28-51. Retrieved from `https://carleton.ca/irrg/journal/`

Beggan, C. D. (2015). Sensitivity of geomagnetically induced currents to varying au-

roral electrojet and conductivity models. *Earth, Planets and Space*, *67*. doi: 10 .1186/s40623-014-0168-9

Beggan, C. D., Beamish, D., Richards, A., Kelly, G. S., & Alan, A. W. (2013). Prediction of extreme geomagnetically induced currents in the UK high-voltage network. *Space Weather*, *11*, 407-419. doi: 10.1002/swe.20065

Boteler, D. H. (2021). Modeling geomagnetic interference on railway signaling track circuits. *Space Weather*, *19*. doi: 10.1029/2020SW002609

Boteler, D. H., & Pirjola, R. J. (2019). Numerical calculation of geoelectric fields that affect critical infrastructure. *International Journal of Geosciences*, *10*, 930-949. doi: 10.4236/ijg.2019.1010053

Boteler, D. H., & Trichtchenko, L. (2015). Telluric influence on pipelines. In R. W. Revie (Ed.), *Oil and gas pipelines: Integrity and safety handbook* (p. 275-288). John Wiley and Sons, Inc. doi: 10.1002/9781119019213.ch21

Cabinet Office. (2012). *National risk register of civil emergencies.* 22 Whitehall, London, SW1A 2WH.

Darch, G., McCormack, L., Hayes, D., Tomlinson, J., Hooper, P., Williams, R., . . . Tyndall, M. (2014). *Rail resilience to space weather final phase 1 report department for transport* (Tech. Rep.). Western House (Block B), Peterborough Business Park, Lynch Wood, Peterborough, PE2 6FZ: Atkins Limited.

Eroshenko, E. A., Belov, A. V., Boteler, D., Gaidash, S. P., Lobkov, S. L., Pirjola, R., & Trichtchenko, L. (2010). Effects of strong geomagnetic storms on northern railways in russia. *Advances in Space Research*, *46*, 1102-1110. doi: 10.1016/j.asr.2010.05.017

Hapgood, M., Angling, M. J., Attrill, G., Bisi, M., Cannon, P. S., Dyer, C., . . . Willis, M. (2021). Development of space weather reasonable worst-case scenarios for the uk national risk assessment. *Space Weather*, *19*. doi: 10.1029/2020SW002593

Iwasaki, M., Furukawa, K., Okamoto, K., Koreishi, K., Kaneyasu, T., Kota, Y., . . . Radford, A. (2017). Development of class 385 semi-customised/standard commuter rolling stock for global markets. *Hitachi Review*, *66*.

Kasinskii, V. V., Ptitsyna, N. G., Lyahov, N. N., Tyasto, M. I., Villoresi, G., & Iucci, N. (2007). Effect of geomagnetic disturbances on the operation of railroad automated mechanisms and telemechanics. *Geomagnetism and Aeronomy*, *47*, 676-680. doi: 10.1134/S0016793207050179

Knight-Percival, A., Johnson, C., Richards, B., Palmer, S., & Bowring, N. (2020). Mapping of the electromagnetic environment on the railway: Condition monitoring of signalling assets. *Proceedings of the Institution of Mechanical Engineers, Part F: Journal of Rail and Rapid Transit*, *234*, 246-256. doi: 10.1177/0954409718802998

Krausmann, E., Andersson, E., Russell, T., & Murtagh, W. (2015). *Space weather and rail: Findings and outlook* (Tech. Rep.). Joint Research Centre, Via E. Fermi 2749, 21027 Ispra (VA), Italy: European Commission. Retrieved from https://ec.europa.eu/jrc doi: 10.2788/211456

Lejdström, B., & Svensson, S. (1956). Calculation of geomagnetic interference voltages in track circuits, original publication (in swedish) appendix 6, betänkande: angående det tekniska utförandet av signalanläggningar vid statens järnvägar, 1956. Translation (in English) June 2020. *Infrastructure Resilience Risk Reporter*, *1*, 28-51. Retrieved from https://carleton.ca/irrg/journal/

Lewis, Z. M., Wild, J. A., Allcock, M., & Walach, M. T. (2022). Assessing the impact of weak and moderate geomagnetic storms on UK power station transformers. *Space Weather*, *20*. doi: 10.1029/2021SW003021

NR/BR/939A. (1971). *Specification for miniature tractive armature ac immune dc neutral track relay, plug-in type for railway signalling purposes* (Tech. Rep.). 40 Melton Street, London, NW1 2EE: Network Rail.

NR/GN/ELP/27312. (2006). *Impedances of 25 kv a.c. overhead lines for classic sys-*

tem (Tech. Rep.). 40 Melton Street, London, NW1 2EE: Network Rail.

NR/SP/ELP/21085. (2007). *Specification for the design of earthing and bonding systems for the 25 kv a.c. electrified lines* (Tech. Rep.). 40 Melton Street, London, NW1 2EE: Network Rail.

NR/SP/SIG/50004. (2006). *Methodology for the demonstration of electrical compatibility with dc (ac immune) track circuits* (Tech. Rep.). 40 Melton Street, London, NW1 2EE: Network Rail.

Patterson, C. J., Wild, J. A., & Boteler, D. H. (2023). Modeling the impact of geomagnetically induced currents on electrified railway signalling systems in the United Kingdom. *Space Weather*. doi: 10.1029/2022SW003385

Patterson et al., 2023(b) model data {Dataset}. (2023). doi: https://doi.org/10.17635/lancaster/researchdata/633

Pirjola, R. (1985). On currents induced in power transmission systems during geomagnetic variations. *IEEE Transactions on Power Apparatus and Systems*, *PAS-104*, 2825-2831. doi: 10.1109/TPAS.1985.319126

Ptitsyna, N. G., Kasinskii, V. V., Villoresi, G., Lyahov, N. N., Dorman, L. I., & Iucci, N. (2008). Geomagnetic effects on mid-latitude railways: A statistical study of anomalies in the operation of signaling and train control equipment on the east-siberian railway. *Advances in Space Research*, *42*, 1510-1514. doi: 10.1016/j.asr.2007.10.015

Pulkkinen, A., Viljanen, A., Pajunpää, K., & Pirjola, R. (2002). Recordings and occurrence of geomagnetically induced currents in the Finnish natural gas pipeline network. *Applied Geophysics*, *48*.

Rogers, N. C., Wild, J. A., Eastoe, E. F., Gjerloev, J. W., & Thomson, A. W. (2020). A global climatological model of extreme geomagnetic field fluctuations. *Journal of Space Weather and Space Climate*, *10*. doi: 10.1051/swsc/2020008

Wik, M., Pirjola, R., Lundstedt, H., Viljanen, A., Wintoft, P., & Pulkkinen, A. (2009). Space weather events in july 1982 and october 2003 and the effects of geomagnetically induced currents on swedish technical systems. *Annales Geophysicae*, *27*, 1775-1787.